

A&A manuscript no.  
(will be inserted by hand later)

Your thesaurus codes are:  
02(02.14.1), 06(06.05.1), 06.09.1, 06.15.1)

ASTRONOMY  
AND  
ASTROPHYSICS

# Solar Models and NACRE thermonuclear reaction rates

P. Morel<sup>1</sup>, B. Pichon<sup>2</sup>, J. Provost<sup>1</sup> and G. Berthomieu<sup>1</sup>

<sup>1</sup> Département Cassini, UMR CNRS 6529, Observatoire de la Côte d'Azur, BP 4229, 06304 Nice CEDEX 4, France

<sup>2</sup> DARC, UMR CNRS 8629, Observatoire de Paris Section Meudon, 92195 Meudon CEDEX, France.

Received date / Accepted date

**Abstract.** Using the most recent updated physics, calibrated solar models have been computed with the new thermonuclear reaction rates of NACRE, the recently available European compilation. Comparisons with models computed with the reaction rates of Caughlan & Fowler (1988) and of Adelberger et al. (1998) are made for global structure, expected neutrinos fluxes, chemical composition and sound speed profiles, helioseismological properties of p-modes and g-modes.

**Key words:** Physical data and processes: nuclear reactions, nucleosynthesis, abundances – Sun: evolution – Sun: interior – Sun: Oscillations

## 1. Introduction

Precise solar models have been constructed over the past three and a half decades (see, e.g. Bahcall et al. 1963; Bahcall 1993, Bahcall et al. 1998b). The refinement have accelerated in the past decade (see, e.g. Bahcall and Ulrich 1988, Bahcall & Pinsonneault 1992b). Since ten years many stellar and solar models have been computed using the thermonuclear reaction rates of Caughlan & Fowler (1988, hereafter C88) a popular compilation but not optimized for solar conditions. More recently some authors (e.g. Bahcall et al. 1995; Reiter et al. 1995; Chaboyer et al. 1995; Berthomieu et al. 1995; Christensen-Dalsgaard et al. 1996) employed the improved thermonuclear reaction rates adopted by Bahcall & Pinsonneault (1992a) for the calculation of accurate solar models. Meanwhile several groups of nuclear physicists have undergone other compilations of updated thermonuclear reaction rates of astrophysical interest. A year ago the compilation of Adelberger et al. (1998, hereafter A98) has been published. The original motivation of this compilation is to assess the state of the nuclear physics important to the solar neutrino problem. The incidences on solar models of these new reaction rates have been analyzed by several groups (see e.g. Bahcall et al. 1998b; Brun et al. 1998; Morel et al. 1998).

Send offprint requests to: P. Morel  
Correspondence to: Pierre.Morel@obs-nice.fr

More recently the European Nuclear Astrophysics Compilation of REaction rates (Angulo et al. 1999, NACRE, hereafter N99) has been completed and opened to free access. The driving motivation of this last work, coordinated by the Institut d'Astronomie et d'Astrophysique of the Université Libre de Bruxelles, is the build-up of well documented and evaluated sets of experimental data or theoretical predictions of astrophysical interest. To have a direct idea of the degree of reliability of any reaction rate, the authors have published, either a very convenient plot of the available measurements of cross section S-factors with respect to energy, or a table showing the range of the various parameters needed for cross section evaluation, e.g. the resonance parameters. Moreover, the accuracy of each analytical fit is indicated. This new compilation gives besides the adopted reaction rate  $\mathcal{R}$ , its lower and upper limits  $\mathcal{R}_l$  and  $\mathcal{R}_u$ . A solar neutrino analysis based on preliminary NACRE data for the PP reactions has been done by Castellani et al. (1997). Recently Arnould et al. (1999) have used the N99 reaction rates to compute abundance predictions in non hydrogen and helium burning. They convincingly show that large spreads in the abundances predictions for several nuclides may result not only from a change in temperature, but also from nuclear physics uncertainties.

We are now in the fortunate position of having two precise and *independent* determinations of the best nuclear fusion data, namely A98 and N99. In order to illustrate the effects, on the standard solar model, of nuclear fusion rates on various astronomical quantities, including neutrino fluxes and helioseismology frequencies, we compare the model results calculated with the best current data from A98 and N99, with results obtained using early estimates of fusion rates of C88. Those differences are not very large. Nevertheless they modify the energy balance, the stratification, the chemical composition and the neutrino generation in the core.

Let us first recall the main constraints known nowadays on solar models. The helioseismological constraints relevant to the core are the small p-mode frequency differences  $\delta\nu_{02}$  and  $\delta\nu_{13}$  and the not yet observed spectrum of gravity modes. Other signatures of changes of

arXiv:astro-ph/9907381v1 27 Jul 1999

**Table 1.** Respectively for the C88, A98 and N99 compilations, the S-factors at zero energy  $S(0)$  (MeV barn) and  $S'(0)$  (barn) are given for each nuclear reaction of solar interest, but  ${}^7\text{Be}(e^-, \nu_{\text{Be}}\gamma){}^7\text{Li}$ . The last column gives  $\Delta\mathcal{R}$ , the global uncertainty of N99's rates computed, for  $T_6 = 15$ , according to Eq. 1. The  $S(0)$  factor of  ${}^{12}\text{C}(p, \gamma){}^{13}\text{N}$  is estimated from the N99 plot.

reactions	C88		A98		N99		$\Delta\mathcal{R}$
	$S(0)$	$S'(0)$	$S(0)$	$S'(0)$	$S(0)$	$S'(0)$	
${}^1\text{H}(p, \beta^+ \nu_{\text{pp}}){}^2\text{H}$	$4.06 \cdot 10^{-25}$	$4.6 \cdot 10^{-24}$	$4.00 \cdot 10^{-25}$	$4.48 \cdot 10^{-24}$	$3.94 \cdot 10^{-25}$	$4.61 \cdot 10^{-24}$	5%
${}^2\text{H}(p, \gamma){}^3\text{He}$	$2.5 \cdot 10^{-7}$	$7.9 \cdot 10^{-6}$			$2.0 \cdot 10^{-7}$	$5.6 \cdot 10^{-6}$	40%
${}^3\text{He}({}^3\text{He}, 2p){}^4\text{He}$	5.56	-8.2	5.4	-4.1	5.18	-2.22	6%
${}^3\text{He}(\alpha, \gamma){}^7\text{Be}$			$5.3 \cdot 10^{-4}$	$-3.0 \cdot 10^{-4}$	$5.4 \cdot 10^{-4}$	$-5.2 \cdot 10^{-4}$	18%
${}^7\text{Li}(p, \alpha){}^4\text{He}$					$5.93 \cdot 10^{-2}$	0.193	14%
${}^7\text{Be}(p, \gamma){}^8\text{B}^*$	$2.39 \cdot 10^{-5}$	0.	$1.9 \cdot 10^{-5}$	$-1.35 \cdot 10^{-5}$	$2.1 \cdot 10^{-5}$	$-1.8 \cdot 10^{-5}$	11%
${}^{12}\text{C}(p, \gamma){}^{13}\text{N}$	$1.40 \cdot 10^{-3}$	$4.2 \cdot 10^{-3}$	$1.34 \cdot 10^{-3}$	$2.6 \cdot 10^{-3}$	$1.5 \cdot 10^{-3}$		11%
${}^{13}\text{C}(p, \gamma){}^{14}\text{N}$	$5.5 \cdot 10^{-3}$	$1.3 \cdot 10^{-2}$	$7.6 \cdot 10^{-3}$	$-7.8 \cdot 10^{-3}$	$7.0 \cdot 10^{-3}$		23%
${}^{14}\text{N}(p, \gamma){}^{15}\text{O}$	$3.2 \cdot 10^{-3}$	$-5.7 \cdot 10^{-3}$	$3.5 \cdot 10^{-3}$	$-1.28 \cdot 10^{-2}$	$3.2 \cdot 10^{-3}$		34%
${}^{15}\text{N}(p, \gamma){}^{16}\text{O}$	$6.4 \cdot 10^{-2}$	$3.2 \cdot 10^{-2}$	$6.4 \cdot 10^{-2}$	$2.1 \cdot 10^{-2}$	$6.4 \cdot 10^{-2}$		23%
${}^{15}\text{N}(p, \alpha){}^{12}\text{C}$	71.	423.	67.5	310.	69.		15%
${}^{16}\text{O}(p, \gamma){}^{17}\text{F}$	$9.3 \cdot 10^{-3}$		$9.4 \cdot 10^{-3}$	$-2.4 \cdot 10^{-2}$	$9.3 \cdot 10^{-3}$		36%
${}^{17}\text{O}(p, \alpha){}^{14}\text{N}$			$9.58 \cdot 10^{-4}$	$1.08 \cdot 10^{-2}$			35%

thermonuclear reaction rates will be the sound velocity profile which is known from inversion of helioseismic data between  $R \gtrsim 0.1 R_\odot$  and  $R \lesssim 0.9 R_\odot$ , and also the radius of the base of the solar convection zone which is precisely located. The amount of observed photospheric depletions of lithium and beryllium which are often ascribed to transport phenomena beneath the convection zone are also sensitive to changes of the thermonuclear reaction rates in their low energy regime. An another constraint also connected to nuclear reaction rates is the isotopic ratio  ${}^3\text{He} / {}^4\text{He}$  measured at present day at the solar surface which is sensitive to the pre-main sequence deuteron burning and to initial isotopic ratios  ${}^2\text{H} / {}^1\text{H}$  and  ${}^3\text{He} / {}^4\text{He}$  of cosmological interest.

The paper is organized as follows: in Sec. 2 in the low energy range, for the nuclear reactions of interest for solar modeling, we summarize the main differences between N99 and A98 with respect to C88. The physics used in the models is described Sec. 3. In Sec. 4 we report results of comparisons between calibrated solar models computed with N99, A98 and C88, finally we conclude in Sec. 5.

## 2. Comparison of thermonuclear reaction rates from N99, A98 and C88 compilations

The most important nuclear reactions relevant of solar modeling are, for the PP chains (Clayton 1968; Bahcall 1989 Table 3.1 and 3.3):

$${}^1\text{H}(p, \beta^+ \nu_{\text{pp}}){}^2\text{H}, {}^2\text{H}(p, \gamma){}^3\text{He}, {}^3\text{He}({}^3\text{He}, 2p){}^4\text{He}, {}^3\text{He}(\alpha, \gamma){}^7\text{Be}, {}^7\text{Be}(e^-, \nu_{\text{Be}}\gamma){}^7\text{Li}, {}^7\text{Li}(p, \alpha){}^4\text{He}, {}^7\text{Be}(p, \gamma){}^8\text{B}^*(\beta^+ \nu_{\text{8B}}){}^8\text{Be}(\alpha){}^4\text{He},$$

and for the CNO bi-cycle:

$${}^{12}\text{C}(p, \gamma){}^{13}\text{N}(\beta^+ \nu_{13\text{N}}){}^{13}\text{C}, {}^{13}\text{C}(p, \gamma){}^{14}\text{N}, {}^{14}\text{N}(p, \gamma){}^{15}\text{O}(\beta^+ \nu_{15\text{O}}){}^{15}\text{N}, {}^{15}\text{N}(p, \gamma){}^{16}\text{O}, {}^{15}\text{N}(p, \alpha){}^{12}\text{C}, {}^{16}\text{O}(p, \gamma){}^{17}\text{F}(\beta^+ \nu_{17\text{F}}){}^{17}\text{O}, {}^{17}\text{O}(p, \alpha){}^{14}\text{N}.$$

Owing to their low termination and small contribution to energetic and nucleosynthesis, despite their interest for neutrino generation, we do not explicitly take into account in the nuclear network  ${}^1\text{H}(pe^-, \nu_{\text{pep}}){}^2\text{H}$  and  ${}^3\text{He}(p, e^+ \nu_{\text{hep}}){}^4\text{He}$  the so-called *pep* and *hep* reactions.

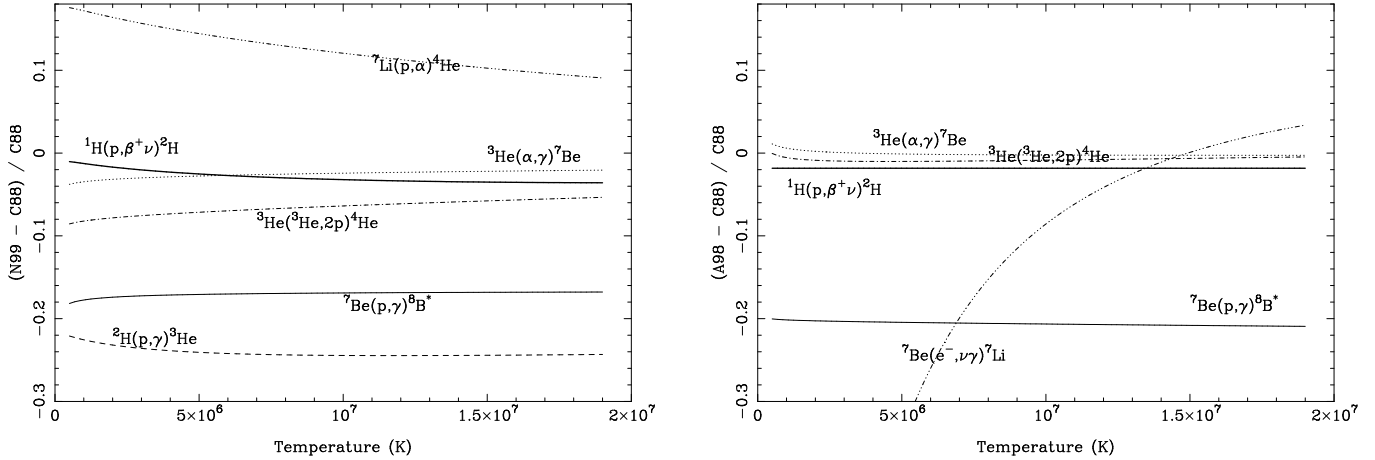


**Fig. 1.** Left panel: relative differences between the reaction rates between N99 and C88 for the relevant solar temperature range  $0.5 \leq T_6 \leq 19$ . for the PP reactions:  ${}^1\text{H}(p, \beta^+ \nu) {}^2\text{H}$  (heavy, full),  ${}^2\text{H}(p, \gamma) {}^3\text{He}$  (dashed),  ${}^3\text{He}({}^3\text{He}, 2p) {}^4\text{He}$  (dot-dash-dot-dash),  ${}^3\text{He}(\alpha, \gamma) {}^7\text{Be}$  (dotted),  ${}^7\text{Li}(p, \alpha) {}^4\text{He}$  (dash-dot-dot-dot) and  ${}^7\text{Be}(p, \gamma) {}^8\text{B}^*$  (thin, full). Right panel: same between A98 and C88.

Nevertheless we compute the number of  $\nu_{\text{pep}}$  neutrino generated using the equation (3.17) of the Bahcall's (1989) reference text book.

The changes between the reaction rates of N99, A98 and C88 are extensively commented in Adelberger et al. (1998) and Angulo et al. (1999). As a matter of illustrations, for the three compilations and for each PP and CNO reaction – but the electronic capture  ${}^7\text{Be}(e^-, \nu_{7\text{Be}} \gamma) {}^7\text{Li}$  – Table 1 gives the S-factors at zero energy and the underlying global uncertainty on the rate  $\Delta \mathcal{R}$ :

$$\Delta \mathcal{R} = \sqrt{\frac{\mathcal{R}_u}{\mathcal{R}_l}} - 1, \quad (1)$$

estimated for  $T_6 = 15$ ;  $T_6$  is the temperature in MK,  $\mathcal{R}_l$  (*resp.*  $\mathcal{R}_u$ ) stands for lower (*resp.* upper) limit of N99 updated reactions. For our thermonuclear reaction network the contributions of resonances to the astrophysical reaction rates are negligible in the solar range of temperatures, therefore the values of  $S(0)$  and, if any,  $S'(0)$  presented here are pertinent. For sake of briefly we omit to reproduce the known  $S''(0)$  values. Figure 1 (*resp.* Fig. 2) compares the relative differences between the adopted rates of N99 (*resp.* A98) and C88 for the temperature range  $0.5 \leq T_6 \leq 19$ .

We next briefly recall the main changes in the rates of A98 and N99, with respect to those of C88 which is the oldest and, up to nowadays, the most used and complete.

${}^2\text{H}(p, \gamma) {}^3\text{He}$ : Among all reactions of PP chains and CNO bi-cycle, it is the rate of this PPI reaction which is the most badly known. The reaction rate is so fast that it is only involved by the pre-main sequence deuteron burning. Owing to the lower value adopted for the S-factors at zero energy, the rate of the reaction which synthesizes  ${}^3\text{He}$  is about  $-24\%$  lower in N99 than in C88. This reaction is not updated in A98, for the calculations with A98 we used the value adopted in C88.

${}^3\text{He}({}^3\text{He}, 2p) {}^4\text{He}$ : For the most energetic reaction of the PP chains N99 (*resp.* A98) adopts values smaller by about  $-6\%$  (*resp.*  $-2\%$ ) than C88 for the S-factors. As consequences of the calibration process, for the models using either N99 or A98, more  ${}^1\text{H}$  nuclear fuel will be burnt in order to reach, at present day, the observed luminosity and effective temperature. Therefore these models will have cores with larger temperature, helium content, density and sound velocity than models computed with C88; then, at first sight, their predicted total neutrino fluxes are expected to be larger. This effect will be enhanced for the models computed with N99 since the rates of the two reactions  ${}^1\text{H}(p, \beta^+ \nu) {}^2\text{H}$  and  ${}^2\text{H}(p, \gamma) {}^3\text{He}$  are smaller in N99 than in C88.

Figure p. 26 of Angulo et al. (1999) gives the impression that, at low energy, the Junker et al.'s (1998) recent measurements are avoided by the interpolation formulae adopted (see also Fig. 2 of Adelberger et al. 1998). These recent data should lead to an increase of  $S(0)$  so, to an enhancement of the efficiency of the reaction and then, owing to the calibration process, to a decrease of solar neutrino fluxes.

${}^7\text{Li}(p, \alpha) {}^4\text{He}$ : The  $S(0)$  value adopted by N99 differs from C88 between  $+15\%$  and  $+7\%$ . In the core its curate rate is irrelevant due, first to its strong rate ( $\approx 10^{-5}$  year, e.g. Bahcall 1989 Table 3.2) and, second to the tiny mass fraction of  ${}^7\text{Li} \sim 2 \cdot 10^{-15}$ . Beneath the convection zone the burning of  ${}^7\text{Li}$  will be more efficient with N99 than with C88, leading to an increase of the lithium depletion at the solar surface at present day. As suggested in C88, the  ${}^7\text{Li}$  burning is slightly enhanced by few percents by the neighbor reaction  ${}^7\text{Li}(p, \gamma) {}^8\text{Be}(\alpha) {}^4\text{He}$  which has been added to our nuclear network. This reaction is not updated in A98, for the calculations with A98 we shall use the value adopted in C88.

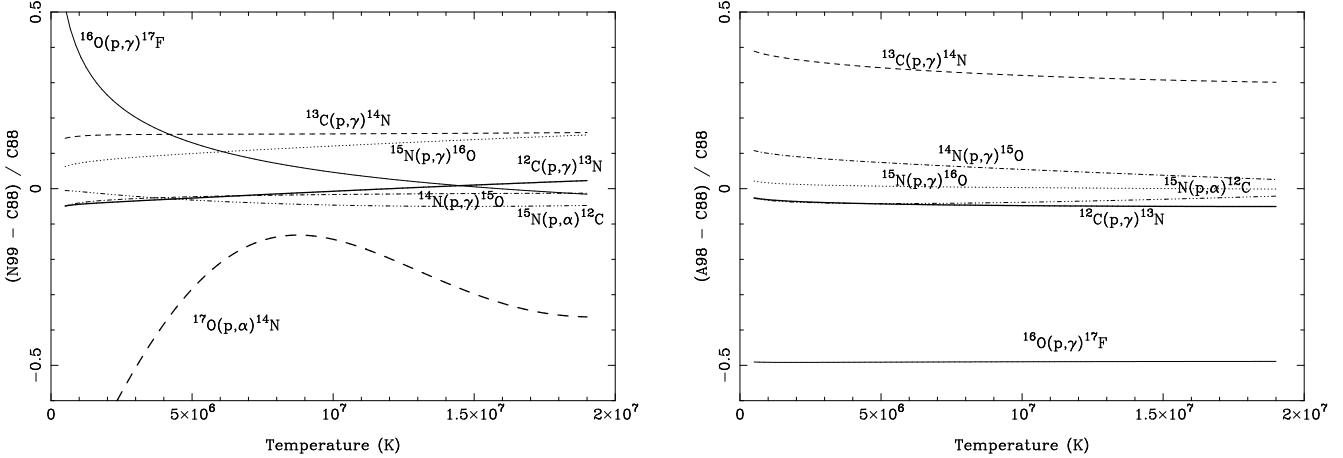


**Fig. 2.** The same as Fig. 1 for the CNO reactions:  $^{12}\text{C}(p, \gamma)^{13}\text{N}$  (heavy, full),  $^{13}\text{C}(p, \gamma)^{14}\text{N}$  (dashed),  $^{14}\text{N}(p, \gamma)^{15}\text{O}$  (dot-dash-dot-dash),  $^{15}\text{N}(p, \gamma)^{16}\text{O}$  (dotted),  $^{15}\text{N}(p, \alpha)^{12}\text{C}$  (dash-dot-dot-dot),  $^{16}\text{O}(p, \gamma)^{17}\text{F}$  (thin, full),  $^{17}\text{O}(p, \alpha)^{14}\text{N}$  (heavy, dashed).

$^7\text{Be}(e^-, \nu_{7\text{Be}}\gamma)^7\text{Li}$ : N99 deals only with charged particle induced reactions involving nuclei, and therefore the  $^7\text{Be}$  electron capture rate is not updated. In the calculations with N99 we shall use the value given by A98. Beneath  $T_6 = 1$  only an upper limit is given in C88 for the  $^7\text{Be}$  electron capture. The adopted rate of A98 differs from the rate of C88 by more than +50% at low temperature; for  $T_6 \sim 15$ , i.e. in the solar core, the rates of C88 and A98 are of same order.

$^7\text{Be}(p, \gamma)^8\text{B}^*$ : This reaction controls the efficiency of the important source of  $\nu_{8\text{B}}$ , the so-called boron solar neutrino. The adopted values for the S-factors at zero energy are slightly larger in N99 than in A98, but still smaller than in C88. With respect to C88, everything else equal, one can expect that the neutrino flux from boron will be reduced for the solar models computed with A98 and N99.

$^{13}\text{C}(p, \gamma)^{14}\text{N}$ : The values of S-factors at zero energy adopted by N99 and A98 are magnified by a factor of about two with respect to their previous values in C88; as a result the rates are increased by +30% and +15% respectively. These large differences will not have any noticeable incidence on the global structure of the core since the energy generated by the CNO bi-cycle is only  $\lesssim 2\%$  of the total nuclear energy.

$^{14}\text{N}(p, \gamma)^{15}\text{O}$ : The rate of the most important reaction for the computation of energy generation and neutrino fluxes created by the CNO bi-cycle is known with a large uncertainty. The three compilations adopt about the same values for the S-factors at zero energy. Figure 2 shows small differences between the rates. This is due to different interpolation formulas which slightly differ since there is no measurement at low energy (see the convincing figure p. 58 of Angulo et al. (1999)).

$^{15}\text{N}(p, \gamma)^{16}\text{O}$ : For the reaction which governs the efficiency of the NO-part of the CNO bi-cycle, N99, A98 and C88 adopt the use of S-factors at zero energy obtained by

Rolfs & Rodney (1974). Due to differences in the interpolation formula Fig. 2 reveals enhanced rates of +15% in N99 with respect to C88 or A98.

$^{16}\text{O}(p, \gamma)^{17}\text{F}$ : At low energy the reaction which controls the generation of  $\nu_{17\text{F}}$ , the so-called fluorine solar neutrino, is based on data with large experimental errors. The adopted rate has the largest uncertainty among the CNO reactions. Though Table 1 gives for the three compilations about the same values for the S-factors, Fig. 2 shows large differences for the rates resulting from different analytical formulations. Beyond  $T_6 \sim 10$ , N99 and C88 are close (Angulo et al. 1999). The difference of -50% between A98 and C88 results of the used of the standard formulation of the non-resonant reaction rate with S-factors (Fowler et al. 1967).

$^{17}\text{O}(p, \alpha)^{14}\text{N}$ : N99 and A98 use different analytical fits based on the measurements of Landré et al. (1989). They differ by -30%. With the discovery of a resonance at low energy (Landré et al. *loc. cit.*) the analytical fit of C88 became in error by more than two order of magnitude. For the models computed with C88 we have used the rates derived from the Landré's et al. analytical fit, as recommended by A98.

*Summary.* With respect to C88 many reaction rates, principally  $^3\text{He}(^3\text{He}, 2p)^4\text{He}$ , are lowered in N99 and also, but in a less extend, in A98. One can expect that this will lead to calibrated solar models with central cores with larger temperature. For the reactions of PP chains, with respect to C88, other important changes connected to the observable neutrino fluxes are the rates of the electronic capture  $^7\text{Be}(e^-, \nu_{7\text{Be}}\gamma)^7\text{Li}$  which is significantly diminished for  $T_6 \lesssim 7$  in A98 and, for N99, the decrease of the rate of  $^7\text{Be}(p, \gamma)^8\text{B}^*$ . With respect to C88, the changes in N99 and A98 of the reaction rates of the CNO bi-cycle are not large enough to modify significantly the solar model.

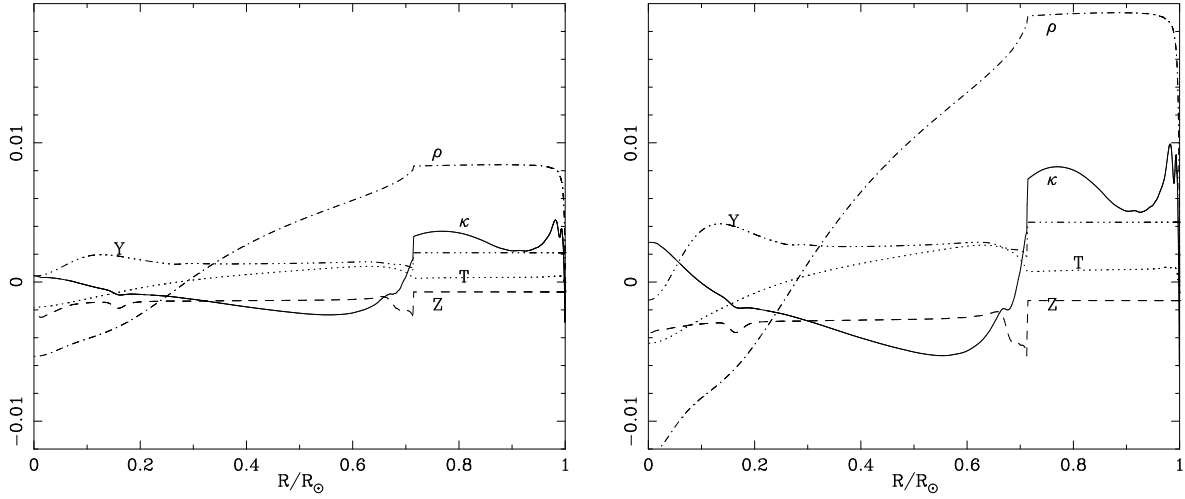


**Fig. 3.** Relative differences in opacity  $\kappa$  (full), heavy element  $Z$  (dashed), density  $\rho$  (dot-dash-dot-dash), temperature  $T$  (dotted) and helium content  $Y$  (dash-dot-dot-dash) for the calibrated models A98 (left) and C88 (right), with respect to model N99.

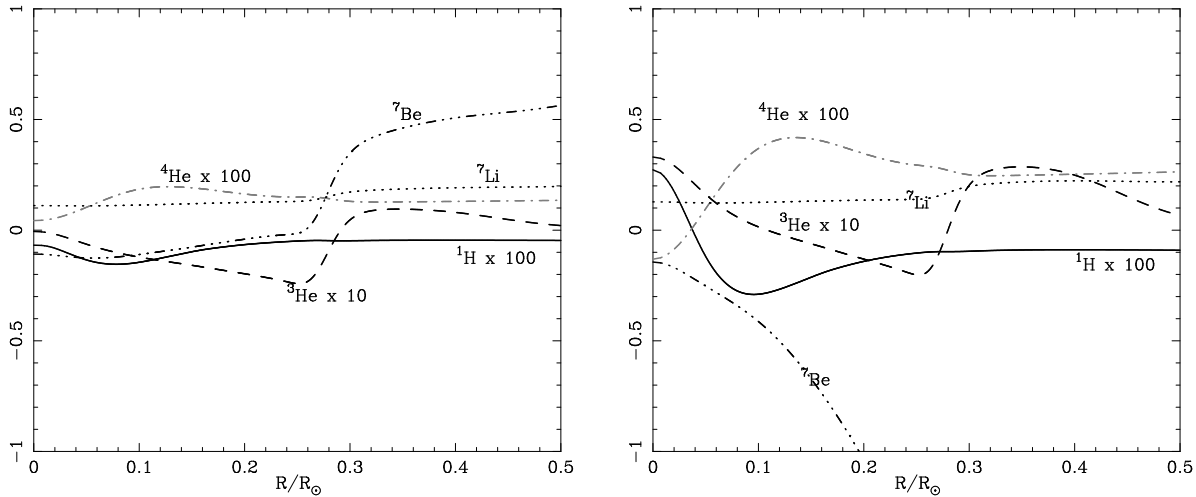


**Fig. 4.** Relative differences of abundances with respect to model N99, for models A98 (left) and C88 (right) for PP species:  ${}^1\text{H} \times 100$  (full),  ${}^3\text{He} \times 10$  (dashed),  ${}^4\text{He} \times 100$  (dash-dot-dash),  ${}^7\text{Li}$  (dotted),  ${}^7\text{Be}$  (dash-dot-dot-dash).

### 3. The solar models

Basically the physics of the models is the same as in Morel et al. (1997).

*Calibration of models.* Each evolution is initialized with a homogeneous zero-age pre-main-sequence model in quasi-static gravitational contraction with the temperature at center  $T_c \sim 0.5$  MK, i.e. close to the onset of the deuterium burning. The models are calibrated within a relative accuracy better than  $10^{-4}$  by adjusting: the ratio  $l/H_p$  of the mixing-length to the pressure scale height, the initial mass fraction  $X_i$  of hydrogen and the initial mass fraction  $(Z/X)_i$  of heavy element to hydrogen in order that, at present day, the solar models have the luminosity  $L_\odot = 3.846 \cdot 10^{33} \text{ erg s}^{-1}$  (Guenther et al. 1992), the radius

$R_\odot = 6.9599 \cdot 10^{10} \text{ cm}$  (Guenther et al. *loc. cit.*) and the mass fraction of heavy element to hydrogen  $(Z/X)_\odot = 0.0245$  (Grevesse & Noels 1993). We used a time of evolution  $t_{\text{ev}} = 4600 \text{ My}$ , an intermediate value between the meteoritic age  $t_{\text{om}} = 4530 \pm 40 \text{ My}$  of the Sun<sup>1</sup> (Guenther 1989) and its helioseismic value  $t_{\text{oh}} = 4660 \pm 100 \text{ My}$  derived by Dziembowski et al. (1998). The zero age main-sequence (ZAMS) is defined as the time where nuclear reactions dominate gravitation as the primary energy source by more than 50% (Guenther et al. *loc. cit.*). The mass of the Sun is assumed to be  $M_\odot = 1.9891 \cdot 10^{33} \text{ g}$  (Cohen & Taylor 1986).

<sup>1</sup> Here  $t_{\text{om}}$  is referenced with respect to ZAMS which occurs  $36 \pm 10 \text{ My}$  (Guenther *loc. cit.*) after the formation of meteorites  $4566 \pm 5 \text{ My}$  from now (Bahcall et al. 1995).

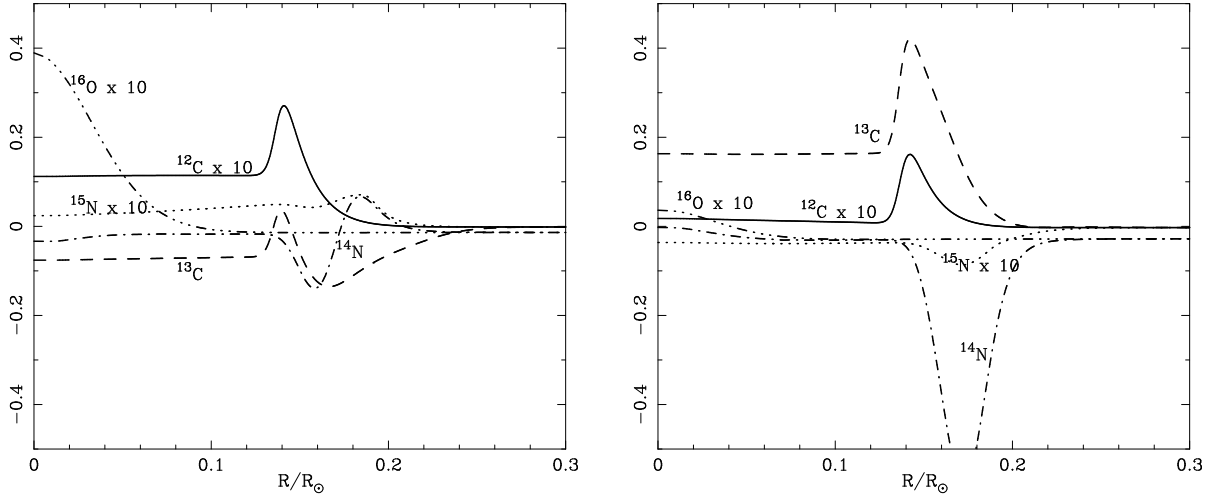


**Fig. 5.** Same as Fig. 4 for the CNO species:  $^{12}\text{C} \times 10$  (full),  $^{13}\text{C}$  (dashed),  $^{14}\text{N}$  (dash-dot-dash-dot),  $^{15}\text{N} \times 10$  (dotted),  $^{16}\text{O} \times 10$  (dash-dot-dot-dash).

*Nuclear and diffusion network.* The general nuclear network we used contains the following species :  $^1\text{H}$ ,  $^2\text{H}$ ,  $^3\text{He}$ ,  $^4\text{He}$ ,  $^7\text{Li}$ ,  $^7\text{Be}$ ,  $^9\text{Be}$ ,  $^{12}\text{C}$ ,  $^{13}\text{C}$ ,  $^{14}\text{N}$ ,  $^{15}\text{N}$ ,  $^{16}\text{O}$ ,  $^{17}\text{O}$  and Ex; Ex is an “Extra” fictitious mean non-CNO heavy element with atomic mass 28 and charge 13 ( $\text{Ex} \sim ^{28}\text{Al}$ ) which complements the mixture i.e.,  $X_{\text{Ex}} = 1 - \sum_{i=^1\text{H}}^{^{17}\text{O}} X_i$  with  $X_i$  as the mass fraction of the species labeled with  $i = ^1\text{H}, \dots, ^{17}\text{O}$ . With respect to time, due to microscopic diffusion processes, the abundances of heavy elements are enhanced toward the center; Ex mimics that enhancement for the non CNO metals which contribute to changes of  $Z$ , then to opacity variations but neither to nuclear energy generation nor to nucleosynthesis. To compute the depletion of  $^9\text{Be}$ , we have added, to the nuclear network given Sec. 2, the most efficient reactions of  $^9\text{Be}$  burning:  $^9\text{Be}(p, d)^2^4\text{He}$  and  $^9\text{Be}(\alpha, n)^{12}\text{C}$ . The life time of the neutron, namely 888s (Barnett et al. 1996), is smaller by more than thirteen orders of magnitude than the evolutionary time scale of the Sun’s main-sequence  $pp$  reaction. Therefore, for the calculations, the last reaction is rewritten  $^9\text{Be}(\alpha, e^- p \bar{\nu}_{^9\text{Be}})^{12}\text{C}$ . The weak screening of Salpeter (1954) is used, it is a very good approximate of the exact solution of the Schrödinger equation for the fundamental  $pp$  reaction (Bahcall et al. 1998a).

The protosolar initial isotopic ratios (in number) for hydrogen and helium are respectively taken as  $^2\text{H}/^1\text{H} = 3.01 \cdot 10^{-5}$ ,  $^3\text{He}/^4\text{He} = 1.1 \cdot 10^{-4}$  (Gautier & Morel 1997). The initial ratios between the heavy elements within  $Z$  are set to their photospheric present day values, namely (in number) C: 0.24551, N: 0.06458 and O: 0.51295 (Grevesse & Noels 1993) then, for the complement Ex: 0.17696. The initial isotopic ratios are derived from the abundances of nuclides (Anders & Grevesse 1989):  $^{13}\text{C}/^{12}\text{C} = 1.11 \cdot 10^{-3}$ ,  $^{15}\text{N}/^{14}\text{N} = 4.25 \cdot 10^{-3}$ ,  $^{17}\text{O}/^{16}\text{O} = 3.81 \cdot 10^{-4}$ . We have used

the meteoritic values (Grevesse & Sauval 1998) for the initial abundances in dex, ( $\text{H} \equiv 12$ ), of Li and Be:

$$\left[ \frac{\text{Li}}{\text{H}} \right] = 3.31 \pm 0.04, \quad \left[ \frac{\text{Be}}{\text{H}} \right] = 1.42 \pm 0.04.$$

For the calculations of depletions, the lithium is assumed to be in its most abundant isotope  $^7\text{Li}$  form, so it is with beryllium assumed to be  $^9\text{Be}$ . Neither the meteoritic abundance nor the nuclide isotopic ratio of  $^7\text{Be}$  are known, due to numerical constraints the protosolar abundance of  $^7\text{Be}$  was somehow arbitrarily taken to a very low, but non zero value, namely  $[^7\text{Be}/^1\text{H}] = -3.58$  dex. The initial abundance of each isotope is derived from isotopic ratios and initial values of  $X \equiv ^1\text{H} + ^2\text{H}$ ,  $Y \equiv ^3\text{He} + ^4\text{He}$  and  $Z/X$  as inferred by the calibration process in order to fulfill the basic relationship  $X + Y + Z \equiv 1$ .

Microscopic diffusion is described by the simplified formalism of Michaud & Proffitt (1993) with each of the heavy elements as a trace element.

*Equation of state, opacities, convection and atmosphere.* We have used the OPAL equation of state (Rogers et al. 1996) and opacities (Iglesias & Rogers 1996) for the solar mixture of Grevesse & Noels (1993) complemented, at low temperatures, respectively by the MHD equation of state (Däppen 1996) and Alexander & Ferguson (1994) opacities. The interpolations of opacities are made with the v9 birational spline package of G. Houdek (Houdek & Rogl 1996; Houdek 1998).

In the convection zones the temperature gradient is computed according to the standard mixing-length theory. The mixing-length is defined as  $l \equiv \alpha H_p$ , where  $H_p$  is the pressure scale height. The convection zones are mixed via a strong turbulent diffusion coefficient, which produces a homogeneous composition.

The atmosphere is restored using a  $T(\tau)$  law derived from an atmosphere model of the Sun computed by van't Veer (1998) with the Kurucz's (1991) ATLAS12 package. The connection with the envelope is made at the Rosseland optical depth  $\tau_b = 20$  (Morel et al. 1994), where the diffusion approximation for radiative transfer becomes valid. A smooth connection of the gradients is insured between the uppermost layers of the envelope and the optically thick convective part of the atmosphere. The radius  $R_\star$  of any model is taken at the optical depth  $\tau_\star \simeq 0.54$  where  $T(\tau_\star) = T_{\text{eff}}$ ; the mass of the star  $M_\star$ , is defined as the mass enclosed in the sphere of radius  $R_\star$ . The external boundary is located at the optical depth  $\tau_{\text{ext}} = 10^{-4}$ , where the density is fixed to its value in the atmosphere model  $\rho(\tau_{\text{ext}}) = 3.55 \cdot 10^{-9} \text{ g cm}^{-3}$ , that corresponds about to the temperature minimum in the solar chromosphere.

*Numerics.* The models have been computed using the CESAM code (Morel 1997). The numerical schemes are fully implicit and their accuracy is first order for the time and third order for the space. For numerical performance and algorithmic constraints the analytical expressions of reaction rates are tabulated with respect to temperature for the range  $0.5 \leq T_6 \leq 20$  and interpolated with a relative accuracy better than  $10^{-5}$ . Each evolution needs about 90 models. Typically 600 mass shell are used along the evolution, it increases up to 2100 for the models used in seismological analysis.

*p-mode and g-mode oscillation calculations.* The frequencies of linear, adiabatic, global acoustic modes of the solar models have been computed for degrees  $\ell = 0$  to  $\ell = 150$  and have been compared to the observations. The characteristic low degree p-mode frequency differences  $\Delta\nu_{n,\ell} = \nu_{n,\ell} - \nu_{n-1,\ell+2}$  for  $\ell = 0$  and  $\ell = 1$ , which provide information on the properties of the solar core, have been fitted by linear regressions with respect to  $n$ :

$$\Delta\nu_{n,\ell} = \delta\nu_{n,\ell} + S_\ell(n - n_0), \quad n_0 = 21, \quad \ell = 0, 1,$$

both for the observations and the theoretical frequencies. For the gravity modes which have not yet been observed, we give the characteristic asymptotic spacing period  $P_0$  according to Provost & Berthomieu (1986).

## 4. Comparison of models

Table 2 gives the global properties of models and Fig. 3 exhibits the profiles, with respect to radius, of the most important variables for the internal structure namely, density, temperature, opacity, helium and heavy element contents.

### 4.1. Chemical composition

The changes in chemical composition directly result from changes of thermonuclear reaction rates but also, in a more

intricate way, from changes in microscopic diffusion coefficients which are sensitive to the temperature and density, and to chemical composition, pressure, temperature and density gradients.

*Changes at the surface and in the envelope.* For the three models N99, A98 and C88, Table 2 shows that the expected photospheric abundances of helium are slightly reduced and remain compatible with the range of observed values. As known (Basu 1997b), the amount of photospheric ‘‘observed’’ helium derived from inversion of helioseismic data is more sensitive to the equation of state than the amount of photospheric ‘‘predicted’’ helium derived from calibrated solar models. Indeed we have calibrated a solar model<sup>2</sup> using C88 thermonuclear reaction rates and the MHD (Däppen 1996) equation of state instead of OPAL and obtained a photospheric helium content  $Y_s = 0.246$  which is the value derived from inversion using the MHD equation of state (Basu & Antia 1995).

Though the  ${}^7\text{Li}$  surface depletion is increased with the use of the enhanced rate of  ${}^7\text{Li}(p, \alpha){}^4\text{He}$  adopted by N99, the predicted abundance is still very far from the observed value. The differences are likely consequences of the lack, in standard solar models, of mixing generated by the shear at the level of the tachocline (see e.g. Gough et al. 1996, Brun et al. 1999). It smoothes the chemical composition gradients and reduces the microscopic diffusion efficiency (Basu 1997a) immediately beneath the convection zone. According to the new observations (Grevesse & Sauval 1998), the predicted photospheric depletion of beryllium is tiny. The predictions for the surface isotopic ratios  $({}^3\text{He}/{}^4\text{He})_s$  by the three models are all within the interval of accuracy given by the observations.

*Changes in the core.* The solar core is the innermost part where the nuclear energy generation is efficient. It extends from the center to about  $R_c \simeq 0.4R_\odot$  slightly beyond the  ${}^3\text{He}$  peak located around  $0.3R_\odot$ . Owing to the less efficiency of PP reactions, see Sec. 2, the temperature, the density, the amount of helium and the sound velocity at center of *calibrated* models N99 and A98, are larger than in C88. As expected, Fig. 4 shows almost symmetrical profiles for the differences for  ${}^1\text{H}$  and  ${}^4\text{He}$ . Owing to the larger efficiency of the *pp* reaction in C88, larger values are obtained for the relative difference C88 minus N99 than for A98 minus N99. The typical features for the relative differences of abundances of  ${}^3\text{He}$  are consequences of the smaller reaction rates of N99 with respect to A98 and C88 of  ${}^3\text{He}({}^3\text{He}, 2p){}^4\text{He}$ . Beneath the  ${}^3\text{He}$  peak, owing to the increase of the temperature, the amount of  ${}^3\text{He}$  is smaller in C88 and A98 than in N99; it is the reverse beyond the peak. Though the same rate prevails in N99 and A98 for the  ${}^7\text{Be}$  electronic capture, there is a non zero value

<sup>2</sup> Not analyzed here for sake of brevity.

**Table 2.** Comparison of global characteristics of solar models computed with the thermonuclear reaction rates of respectively Angulo et al. (1999, N99), Adelberger et al. (1998, A98) and Caughlan & Fowler (1988, C88) compilations. The first four rows give the initial values of  $Y_i$  (*resp.*  $Z_i$ ) the mass fraction of helium (*resp.* heavy element),  $(Z/X)_i$  the mass fraction of heavy element to hydrogen,  $\alpha$  the mixing-length parameter.  ${}^7\text{Li}_{sz}$  (*resp.*  ${}^9\text{Be}_{sz}$ ) and  ${}^7\text{Li}_s$  (*resp.*  ${}^9\text{Be}_s$ ) respectively are the surface depletions in dex ( $H \equiv 12$ ) of  ${}^7\text{Li}$  (*resp.*  ${}^9\text{Be}$ ) at zero-age main sequence and at present day. All other item are for present day. The surface isotopic ratio  $({}^3\text{He}/{}^4\text{He})_s$  is in unit of  $10^{-4}$ ;  $Y_s$ ,  $Z_s$  respectively are the surface mass fraction of helium and heavy element;  $R_{CZ}$  is the radius, in solar units, at the bottom of the convection zone;  $T_c$ ,  $\rho_c$ ,  $Y_c$  and  $Z_c$  are the central values respectively of, the temperature in units of  $10^7\text{K}$ , the density in  $\text{g cm}^{-3}$ , the mass fraction, of helium and heavy element.  $\delta\nu_{02}$  and  $\delta\nu_{13}$  are the values, in  $\mu\text{Hz}$ , of the frequency differences between the radial p-modes of degree  $\ell = 0 - 2$  and  $\ell = 1 - 3$ .  $P_0$  is the characteristic spacing period of g-modes in minutes.

	N99	A98	C88	Observed values
$Y_i$	0.2723	0.2726	0.2729	
$Z_i$	0.0197	0.0197	0.0196	
$(Z/X)_i$	0.0278	0.0278	0.0277	
$\alpha$	1.924	1.931	1.941	
${}^7\text{Li}_{sz}$	2.26	2.38	2.37	
${}^9\text{Be}_{sz}$	1.42	1.42	1.42	
${}^7\text{Li}_s$	2.18	2.30	2.29	$1.10 \pm 0.10$ , Grevesse & Sauval (1998)
${}^9\text{Be}_s$	1.35	1.35	1.353	$1.40 \pm 0.09$ , Grevesse & Sauval (1998)
$({}^3\text{He}/{}^4\text{He})_s$	4.34	4.32	4.32	$4.4 \pm 0.4$ , Bodmer et al. (1995)
$Y_s$	0.2436	0.2442	0.2447	$0.232 - 0.249$ , Basu (1997b)
$Z_s$	0.0181	0.0181	0.0181	
$R_{CZ}$	0.7138	0.7132	0.7124	$0.713 \pm 0.001$ , Basu & Antia (1995)
$T_c$	1.573	1.570	1.566	
$\rho_c$	153.8	153.0	151.9	
$Y_c$	0.6418	0.6420	0.6409	
$Z_c$	0.0210	0.0210	0.0210	
$\delta\nu_{02}$	9.21	9.18	9.16	$9.002 \pm 0.044 - 9.014 \pm 0.042$ , from LOI/GOLF (see text)
$\delta\nu_{13}$	16.10	16.06	16.03	$15.884 \pm 0.034 - 15.711 \pm 0.071$ , from LOI/GOLF (see text)
$P_0$	35.13	35.23	35.42	

for relative difference between the  ${}^7\text{Be}$  profiles of models N99 and A98, resulting of differences between the rates adopted for  ${}^3\text{He}(\alpha, \gamma){}^7\text{Be}$ .

Figure 5 exhibits large differences in the abundances of  ${}^{16}\text{O}$  for A98 and C88 with respect to N99 despite the fact that the rates of the reactions of  ${}^{16}\text{O}$  burning are close. In fact, these differences result from changes of rates of  ${}^{15}\text{N}$  burning which creates  ${}^{16}\text{O}$ . For  ${}^{12}\text{C}$  and  ${}^{14}\text{N}$ , around  $0.18R_\odot$ , effects of changes of nuclear reaction rates are magnified by the large gradients of that species. There, Fig. 3 reveals, on  $Z$  profiles, small bumps due to the magnification by large gradients of variations in chemical composition caused by the changes of thermonuclear reaction rates.

#### 4.2. Thickness of the convection zone.

For radius  $R \gtrsim 0.4R_\odot$ , i.e. in the envelope, Fig. 3 shows that the opacity profiles are close within  $\pm 0.4\%$  for models N99 and A98. The thickness of the convection zone is about the same in N99 and A98, and close, within the error bars (see Table 2), to the observed value. It is slightly larger for model C88. That difference is due to the increase of the radiative temperature gradient resulting from the higher value of the opacity. The differences of temperature between N99 and A98 being small, the changes in opacity are mainly due to the variations of density. The relative opacity differences amount to  $\pm 1\%$  between C88 and N99.

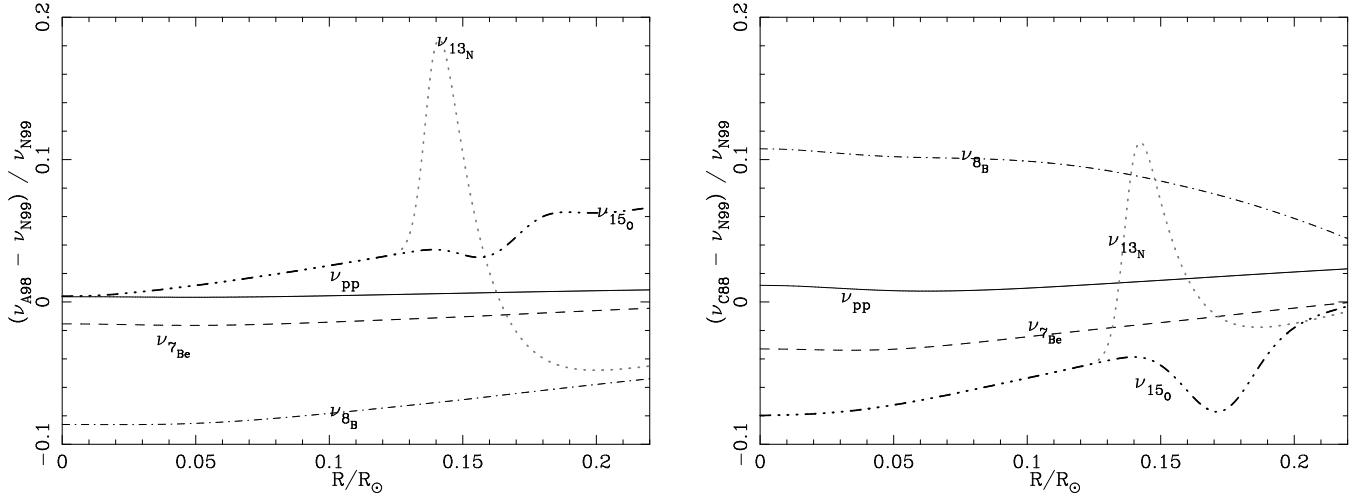


**Fig. 6.** Left panel: relative differences of neutrino rates generation, between models A98 and N99, for  $\nu_{pp}$  (thin, full),  $\nu_{7\text{Be}}$  (dashed),  $\nu_{8\text{B}}$  (dot-dash-dot-dash),  $\nu_{13\text{N}}$  (dotted),  $\nu_{15\text{O}}$  (dash-dot-dot-dash). Right panel: the same between models C88 and N99

**Table 3.** The same as Table 2 for the neutrino fluxes. Using the comprehensive symbols, defined Sec. 2,  $\nu_{pp}$ ,  $\nu_{pep}$ ,  $\nu_{7\text{Be}}$ ,  $\nu_{8\text{B}}$ ,  $\nu_{13\text{N}}$ ,  $\nu_{15\text{O}}$ ,  $\nu_{17\text{F}}$  are, at earth level, the number  $\text{cm}^{-2} \text{s}^{-1}$  of neutrinos of each kind.  $\Phi_{\text{Ga}}$  and  $\Phi_{\text{Cl}}$  in SNU and  $\Phi_{\text{Ka}}$  in events  $\text{day}^{-1}$ , are the expected fluxes for the three neutrino experiments namely gallium, chlorine and Kamiokande (see text). The observed values for  $\Phi_{\text{Ga}}$ ,  $\Phi_{\text{Cl}}$  and  $\Phi_{\text{Ka}}$  are respectively from Hampel et al. (1999), Davis (1994) and Fukuda et al. (1996).

	N99	A98	C88	Observed values
$\nu_{pp}$	$5.91 \cdot 10^{10}$	$5.92 \cdot 10^{10}$	$5.94 \cdot 10^{10}$	
$\nu_{pep}$	$1.40 \cdot 10^8$	$1.40 \cdot 10^8$	$1.48 \cdot 10^8$	
$\nu_{7\text{Be}}$	$4.90 \cdot 10^9$	$4.80 \cdot 10^9$	$4.71 \cdot 10^9$	
$\nu_{8\text{B}}$	$5.68 \cdot 10^6$	$5.17 \cdot 10^6$	$6.19 \cdot 10^6$	
$\nu_{13\text{N}}$	$5.73 \cdot 10^8$	$5.77 \cdot 10^8$	$5.34 \cdot 10^8$	
$\nu_{15\text{O}}$	$4.96 \cdot 10^8$	$5.01 \cdot 10^8$	$4.57 \cdot 10^8$	
$\nu_{17\text{F}}$	$6.41 \cdot 10^6$	$3.15 \cdot 10^6$	$5.74 \cdot 10^6$	
$\Phi_{\text{Ga}}$	130.1	128.4	129.8	$77.75 \pm 6.2^{+4.3}_{-4.7}$
$\Phi_{\text{Cl}}$	8.31	7.71	8.82	$2.55 \pm 0.25$
$\Phi_{\text{Ka}}$	0.61	0.55	0.66	$0.29 \pm 0.02$

### 4.3. Neutrinos

Table 3 gives the predicted neutrino fluxes at earth level and the expected fluxes for the three neutrino experiments namely, chlorine (e.g. Davis 1994), gallium (e.g. Hampel et al. 1999) and Kamiokande (e.g. Fukuda et al. 1996), computed according to Berthomieu et al. (1993). The gallium and chlorine absorption cross sections have been taken respectively from Bahcall (1997) and Bahcall et al. (1996).

The *hep* flux which may be important (e.g. Bahcall & Krastev 1998c, Fiorentini et al. 1998) in the neutrino spectrum measurements by the SuperKamiokande, SNO and Icarus experiments is not listed. With respect to C88, due to hotter core,  $\nu_{7\text{Be}}$  and CNO neutrino fluxes are enhanced in A98 and N99 and, as expected,  $\nu_{pp}$  is slightly reduced.

Despite larger temperatures in the core we obtained, for the models A98 and N99 with respect to the model C88, the expected decreases of the  $\nu_{8\text{B}}$  boron neutrino fluxes owing to their reduced rate of the reaction  ${}^7\text{Be}(p, \gamma){}^8\text{B}^*$ . The introduction of N99 reaction rates relatively to A98 induces an increase of +10% of  $\nu_{8\text{B}}$ . The effect is significant on the flux measured by the chlorine and Kamiokande experiments. Note that Table 3 reveals that the neutrino fluxes at earth level for A98 are very similar than those given Table 1 in Bahcall et al. (1998b). They differ only by few percent for  $\nu_{17\text{F}}$  owing to the large abundance of  ${}^{16}\text{O}$  resulting from the great efficiency of  ${}^{15}\text{N}$  burning which about double the fraction of termination of the NO part of the CNO bi-cycle. Despite the fact that the two stellar evolution programs are entirely independent of each other, when the same nuclear reaction rates are used (A98), the most important neutrino fluxes  $\nu_{pp}$ ,  $\nu_{pep}$ ,  $\nu_{7\text{Be}}$ ,  $\nu_{8\text{B}}$ ,  $\nu_{13\text{N}}$ , and  $\nu_{15\text{O}}$  all agree to better than 1%.

### 4.4. Seismological comparison

The seismic properties of the solar model are mainly related to the profile of sound-speed (*resp.* Brunt-Väissälä frequency) as far as p-modes (*resp.* g-modes) are concerned. Figure 7 shows that the models N99 and, to a lesser extend A98, compared to C88, have a larger sound speed in the central core below 0.3 solar radius by +0.2% (*resp.* +0.1%), and a smaller one by -0.1% (*resp.* -0.05%) just below the convection zone. Table 2

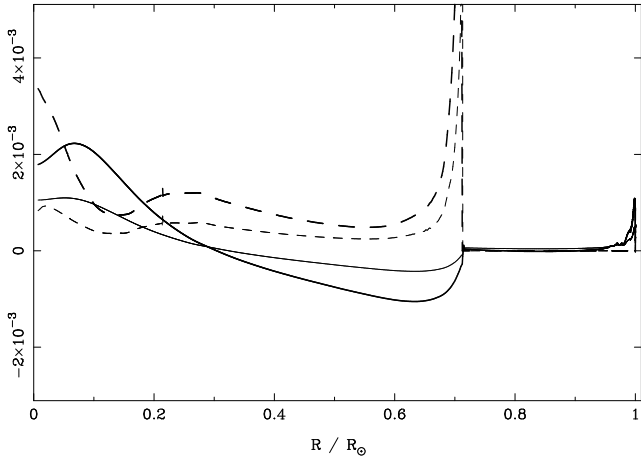


**Fig. 7.** Relative frequency differences of sound speed (full) and square of Brunt-Väissälä frequency divided by 10 (dashed) between N99 (thick) and C88, and A98 (thin) and C88.

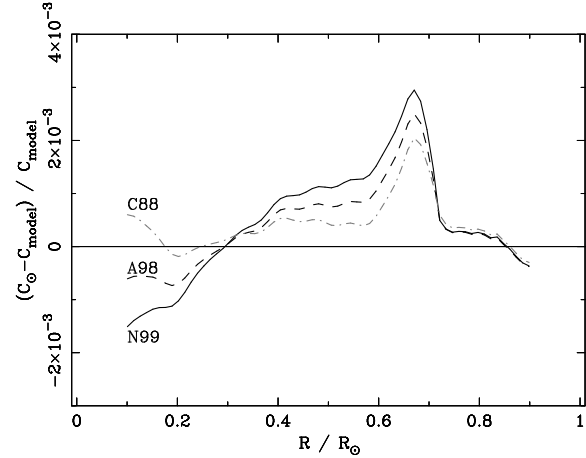


**Fig. 9.** Relative difference in sound velocity between the Sun and the calibrated models N99 (full), A98 (dashed) and C88 (dot-dash-dot-dash).

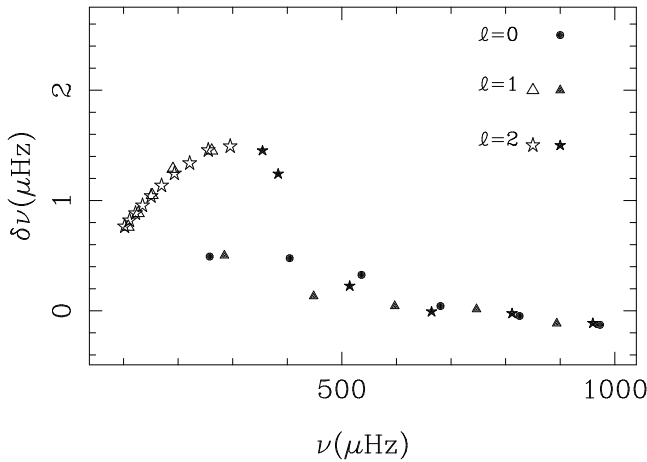


**Fig. 8.** Frequency differences (in  $\mu\text{Hz}$ ) in the low frequency range between N99 and C88 for modes of degree  $\ell = 0, 1, 2$ . Open symbols denote g-modes and, full symbols, f-modes and p-modes.

shows a small increase of small low degree differences  $\delta\nu_{02}$  and  $\delta\nu_{13}$ , as defined Sec. 3 in relation with the difference of sound speed in the solar core. There the relative differences in the Brunt-Väissälä frequency between models N99 and C88 are larger by a few percents, i.e. one order of magnitude larger than the sound speed differences. The increase of the Brunt-Väissälä frequency leads to a  $-1\%$  smaller value of  $P_0$ , the characteristic spacing period of g-modes. The differences between A98 and C88 are three times smaller. This change in Brunt-Väissälä frequency influences much the low frequency modes for frequency less than 1 mHz, i.e. the low radial order p-modes, the f- and g-modes. Consequently the frequency differences of the low degree p-modes between models N99 and C88 vary from  $-0.1 \mu\text{Hz}$  to  $-0.25 \mu\text{Hz}$  when the frequency increases from 1 mHz to 5 mHz, with a minimum value of  $-0.5 \mu\text{Hz}$

around 2 mHz. The normalized frequencies differences for p-modes of degree  $\ell = 3$  to  $\ell = 150$  are negative and change by less than  $-1 \mu\text{Hz}$  in the observed range. As expected, the change of nuclear reaction rates do not modify the frequency of oscillation of degree larger than 70.

Figure 8 shows the frequencies differences in low frequency range between N99 and A98 and Table 4 gives the frequencies of g- and p-modes for  $\ell = 0$  to  $\ell = 2$  in the same frequency range. In the low frequency range  $400 \mu\text{Hz} - 1 \text{ mHz}$ , it appears that the p-mode frequencies are changed by less than  $0.5 \mu\text{Hz}$  between N99 and C88, i.e. by less than  $+0.1\%$ , with an effect larger at lower frequency. Below  $200 \mu\text{Hz}$ , the oscillations are gravity modes with an asymptotic behavior, and the relative period differences are almost proportional to  $P_0$  given in Table 4 (see Provost et al. 1998 for details). Between 200 to  $400 \mu\text{Hz}$ , the oscillations are gravity modes, or f- and p1-modes and they are more influenced by the change of the Brunt-Väissälä frequency in the solar core, induced by changes in nuclear reactions, except the p1-modes for  $\ell = 0$  and  $\ell = 1$ . Frequencies shifts are much larger, of the order of 1 to  $1.5 \mu\text{Hz}$ , when the frequency varies from  $200 \mu\text{Hz}$  to  $400 \mu\text{Hz}$ , i.e. about  $1\%$ , when comparing the models N99 and C88.

In the range  $0.1 R_\odot \lesssim R \lesssim 0.9 R_\odot$  where the inversions of the helioseismic data are reliable, the sound speed of the three models has been compared with the seismic sound speed experimental results of Turck-Chièze et al. (1997). Figure 9 shows that the relative differences are below a few  $10^{-3}$ . The discrepancy between the Sun and the models is larger for model N99 with sound speed too small just below the convection zone and too large in the core. Table 2 shows that it is the same for the quantities  $\delta\nu_{02}$  and  $\delta\nu_{13}$  of the models compared to the corresponding observed values  $\delta\nu_{n,\ell}$  derived from GOLF (Grec et al.

**Table 4.** Frequency of g-modes and p-modes in the range 100  $\mu$ Hz–2 mHz.  $\mathcal{T}$  is the type of the mode labelled by the radial order.

$\ell$	C88	N99	$\mathcal{T}$	$\ell$	C88	N99	$\mathcal{T}$
0	257.82	258.31	p1	2	101.88	102.64	g10
	404.32	404.79	p2		111.07	111.88	g9
	535.98	536.30	p3		121.91	122.80	g8
	680.67	680.71	p4		134.87	135.82	g7
	825.56	825.52	p5		150.51	151.55	g6
	972.95	972.82	p6		169.69	170.83	g5
	1118.36	1118.15	p7		193.24	194.49	g4
	1263.78	1263.60	p8		221.23	222.57	g3
	1407.86	1407.58	p9		255.22	256.67	g2
	1548.78	1548.51	p10		295.44	296.93	g1
	1687.12	1686.81	p11		354.60	356.06	f
	1822.51	1822.14	p12		383.36	384.60	p1
	1957.79	1957.44	p13		514.35	514.58	p2
1	108.55	109.31	g5	811.77	811.75	p3	
	127.04	127.93	g4	959.86	959.75	p4	
	152.45	153.50	g3	1105.18	1105.01	p5	
	190.56	191.85	g2	1250.78	1250.60	p6	
	261.62	263.07	g1	1394.73	1394.46	p7	
	284.77	285.27	p1	1536.06	1535.80	p8	
	448.34	448.48	p2	1674.78	1674.44	p9	
	596.90	596.95	p3	1810.37	1810.01	p10	
	746.65	746.66	p4	1946.00	1945.63	p11	
	893.71	893.60	p5			p12	
	1039.63	1039.52	p6				
	1185.68	1185.47	p7				
	1329.80	1329.57	p8				
	1473.13	1472.88	p9				
	1612.86	1612.53	p10				
	1749.57	1749.25	p11				
	1885.34	1884.94	p12				

1997) and VIRGO/LOI (Fröhlich et al. 1997) observations on SoHO.

## 5. Discussion and conclusions

We have compared the structure, the neutrino fluxes, the chemical composition profiles and the helioseismological properties of calibrated standard solar models computed with the adopted nuclear reaction rates of the European compilation NACRE (Angulo et al. 1999) with those of calibrated solar models computed with the nuclear reaction rates of Caughlan & Fowler (1988) and Adelberger et al. (1998).

Roughly speaking, the thermonuclear reaction rates of PP chains adopted by NACRE and, but in less extend, by Adelberger et al., are slightly less efficient than those adopted by Caughlan & Fowler. The calibration generates models with cores of larger temperature, density, helium

content and sound speed with the concomitant increase of the neutrino fluxes, except for  $\nu_{pp}$  and  $\nu_{sB}$ ; for this last one, the decrease is due to the smaller rate of the reaction  ${}^7\text{Be}(p, \gamma){}^8\text{B}^*$ . Thus the predicted neutrino fluxes are reduced for the chlorine and Kamiokande experiments, but almost unchanged for gallium. For Kamiokande and chlorine, N99 predicts intermediate values between A98 and C88.

The introduction of the NACRE thermonuclear rates increases the discrepancy between predicted and observed sound velocity profiles between the Sun and the models, both below the convection zone and in the solar core. These relative differences, though at the level of a few thousandths, are smaller for the model computed with the reaction rates of Caughlan & Fowler, the increase is  $\sim +0.5\%$  for C98 and  $\sim +1\%$  for N99. The radius at the base of the solar convection zone is in good agreement with the observed value for all models.

Though NACRE adopts an enhanced rate for the reaction of lithium burning  ${}^7\text{Li}(p, \alpha){}^4\text{He}$ , the predicted depletion of photospheric lithium remains too small to fit the observed value.

The differences between calibrated solar models computed with the adopted thermonuclear reaction rates of the two new compilations are rather small. It is not really possible to make any choice between them. From an increase of the accuracy of the observed p-mode frequencies and from a hopefully detection of g-modes one can expect to improve our knowledge on the stratification of the solar core in the goal to validate, in the low energy regime, the thermonuclear reaction rates and their concomitant neutrino generation.

Thanks are due to the NACRE’s work which also provides these estimates of uncertainties on the adopted rates. These new features, now available to the user, are important to constraint the solar model. We are investigating this point in a work in progress.

*Acknowledgements.* It is a pleasure to thank the referee Pr. J.N. Bahcall for bringing several references to our attention, helping us to clarify several points and making several constructive suggestions which have improved the paper. This work has been performed using the computing facilities provided by the OCA program “Simulations Interactives et Visualisation en Astronomie et Mécanique (SIVAM)”. W. Däppen is acknowledged for kindly providing the MHD package of equation of state.

## References

- Adelberger E. G., Austin S. M., Bahcall J.N. et al., 1998, Rev. Mod. Phys. 70, 4, 1265
- Alexander D.R., Fergusson J.W., 1994, ApJ 437, 879
- Angulo C., Arnould M., Rayet M. and the NACRE collaboration 1999, Nuclear Physics A Special issue, in press, and Web site <http://pntpm.ulb.ac.be/Nacre/nacre.htm>
- Anders E., Grevesse N., 1989, Geochimica et Cosmochimica Acta 53, 197

- Arnould M., Goriely S., Jorissen A., 1999, *A&A* 347, 572
- Bahcall J.N., Fowler W.A.; Iben I.Jr., Sears R.L., 1963, *ApJ* 137, 344
- Bahcall J.N., Ulrich R.K., 1988, *Rev. Mod. Phys.* 60, 297
- Bahcall J.N., 1989, *Neutrino Astrophysics* Cambridge University Press
- Bahcall J.N., Pinsonneault M.H., 1992a, *Rev. Mod. Phys.* 60, 297
- Bahcall J.N., Pinsonneault M.H., 1992b, *ApJ* 395, L119
- Bahcall J.N., 1993, *Solar Neutrinos: What We Have Learned*. In: Roxburg I.W. and Masnou J.-L. (eds.) *Physical Processes in Astrophysics, Proceedings of a Meeting in Honour of Evry Schatzman. Lecture Notes in Physics* Springer-Verlag Berlin Heidelberg 1995, p. 19
- Bahcall, J.N., Pinsonneault, M.H., Wasserburg, G.J. 1995, *Rev. Mod. Phys.* 67, 781
- Bahcall J.N., Lisi E., Alburger D.E., De Braeckeleer L., Freedmann J.S., Napolitano J., 1996, *Phys. Rev. C* 54, 411
- Bahcall J.N., 1997, *Phys. Rev. C* 56, 3391
- Bahcall J.N., Chen X., Kamionkowski M., 1998a, *Phys. Rev. C* 57, 2756
- Bahcall J.N., Basu S., Pinsonneault M.H., 1998b, *Phys. Lett. B* 433, 1
- Bahcall J.N., Krastev P.I., 1998, *Phys. Lett. B* 436, 243
- Barnett R.M., et al., 1996, *Phys. Rev. D* 54, 1
- Basu S., Antia H.M., 1995, *MNRAS* 276, 1402
- Basu S., 1997a, *MNRAS* 288, 572
- Basu S., 1997b, *The seismic Sun* In: Provost J., Schmitter F.X. (eds.) *Sounding solar and stellar interiors*, IAU Symposium 181, Kluwer Academic Publishers, p. 137
- Berthomieu G., Provost J., Morel P., Lebreton Y., 1993, *A&A* 268, 775
- Berthomieu G., Provost J., Morel P., 1995, *Neutrino capture rates predicted by standard solar models*. In: Ulrich R.K., Rhodes E. J., Däppen W. (eds.) *GONG94 Helio and Asteroseismology from earth and space ASP Conf. Series* 76, 109
- Brun A.S., Turck-Chièze S., Morel P., 1998, *ApJ* 506,913
- Brun A.S., Turck-Chièze S., Zahn J.P., 1999, *ApJ* in press and [astro-ph/9906382](http://astro-ph/9906382)
- Bodmer R., Bochsler P., Geiss J., von Steiger R., Gloecker G., 1995, *Space Sci. Rev.* 72, 61
- Caughlan G.R., Fowler W.A., 1988, *Atomic Data and Nuclear Data Tables* 40, 284
- Chaboyer B., Demarque P., Pinsonneault M.H., 1995, *ApJ* 441, 865
- Christensen-Dalsgaard J., Däppen W., Ajukov S.V., 1996, *Sciences* 272, 1286
- Castellani V., Degl'Innocenti S., Fiorentini G., Lisia M., Ricci B., 1997, *Phys. Rep.* 281, 309
- Clayton D.D., 1968, *Principles of Stellar Evolution and Nucleosynthesis*, Mc Graw-Hill
- Cohen E.R., Taylor B.N., 1986, *Codata Bulletin* No. 63, Pergamon Press New York
- Davis R. Jr., 1994, *Prog. Part. Nucl.* 32, 13
- Däppen W., 1996 *Bull. Astron. Soc. India* 24,151
- Dziembowski W.A., Fiorentini G., Ricci, B., Sienkiewicz R., 1998, *A&A* in press, and [astro-ph/9809361](http://astro-ph/9809361)
- Fiorentini G., Berezinsky V., Deg'Innocenti S., Ricci B., 1998, [astro-ph/9810083](http://astro-ph/9810083)
- Fowler W.A., Caughlan G.R., Zimmerman B.A., 1967, *ARA&A* 5, 523
- Fröhlich C., Andersen B.N., Appourchaux T., et al., 1997, *First results from VIRGO on SoHO*. In: Provost J., Schmitter F.X. (eds.) *Sounding solar and stellar interiors*, IAU Symposium 181, Kluwer Academic Publishers, 67
- Fukuda, Y. and the Kamiokande Collaboration, 1996, *Phys. Rev. Lett.* 77, 1683
- Gautier D., Morel P., 1997, *A&A* 323, L9
- Gough D.O., Kosovichev A.G., Toomre J., et al., 1996, *Sciences* 272,1296
- Grec G., Turck-Chièze S., Lazrek M., et al., 1997, *GOLF results: today's view on the solar modes*. In: Provost J., Schmitter F.X. (eds.) *Sounding solar and stellar interiors*, IAU Symposium 181, Kluwer Academic Publishers, 91
- Grevesse N., Noels A., 1993, *Cosmic Abundances of the Elements*. In: Prantzos N., Vangioni-Flam E., Casse M. (eds.) *Origin and Evolution of the Elements*. Cambridge University Press, 14
- Grevesse N., Sauval A.J., 1998, *Standard Solar Composition*. In: Fröhlich C., Huber M.C.E., Solanki S.K., Von Steiger R. (eds.) *Solar Composition and its Evolution - from Core to Corona*, ISSI workshop, Space Sciences Series of ISSI 5, 161
- Guenther D.B., 1989, *ApJ* 339, 1156
- Guenther D.B., Demarque P., Kim Y.C., Pinsonneault M.H., 1992, *ApJ*, 387, 372
- Hampel W., Handt J., Heusser G. and the GALLEX collaboration, 1999, *Phys. Lett. B* 447, 127
- Houdek G., Rogl J., 1996, *Bull. Astr. Soc. India* 24, 317
- Houdek G., 1998, *v9 opacities package taken from the WEB site* [ftp://solaris.tuwien.ac.at/incoming/](http://solaris.tuwien.ac.at/incoming/)
- Iglesias C.A., Rogers F.J., 1996, *ApJ* 464, 943
- Junker M., D'Alessandro A., Zavatarelli S., et al., 1998, *Phys. Rev. C* 57, 2700
- Kurucz R.L., 1991, *Stellar Atmospheres: Beyond Classical Models*. In: Crivally L., Hibeny I. and Hammer D.G. (eds.), *NATO ASI Series*, Kluwer, Dordrecht
- Landré V., Aguer P., Bogaert G. et al., 1989, *Phys. Rev. C* 40, 1972
- Michaud G., Proffitt C.R., 1993, *Particule Transport Process*. In: Baglin A., Weiss W.W. (eds.) *Inside the Stars*, IAU Colloquium 137, ASP Conference Series, Vol. 40, 246
- Morel P., van't Veer C., Provost J. Berthomieu G., Castelli F., Cayrel R., Lebreton Y. 1994, *A&A*, 286, 91
- Morel P., 1997, *A&AS* 124, 597
- Morel P., Provost J., Berthomieu G., 1997, *A&A* 327, 349
- Morel P., Provost J., Berthomieu G., 1998, *How solar models fit the SoHO observations?* In: A. Wilson (ed.) *SOHO6/GONG98: Structure and Dynamics of the Interior of the Sun and Sun-like Stars*, ESA Publication SP-418, p. 499
- Provost J., Berthomieu G., 1986, *A&A* 165, 218
- Provost J., Berthomieu G., Morel P., 1998, *Sensitivity of low frequency oscillations to updated solar models*. In: C. Fröhlich, M.C.E. Huber, S. Solanki and R. von Steiger (eds) *Solar composition and its evolution - From Core to Corona*, *Space Science Reviews* 85, p. 117
- Rogers F.J., Swenson F.J., Iglesias C.A., 1996, *ApJ* 456, 902
- Reiter J., Walsh L., Weiss A., 1995, *MNRAS* 274, 899
- Rolfs C., Rodney W.S., 1974, *Nucl. Phys A* 235, 450
- Salpeter E.E., 1954, *Australian J. Phys.* 7, 373
- Turch-Chièze S., Basu S., Brun S., et al., 1997, *Solar Phys.* 175, 247
- van't Veer C., 1998, private communication